Journal of Polymer Research (2020) 27: 138
https://doi.org/10.1007/s10965-020-02120-6

ORIGINAL PAPER

Synthesis of poly (hexamethylene terephthalamide) -co-polycaprolactam/modified montmorillonite nanocomposites with enhanced mechanical properties and lower water absorption rate by in-situ polymerization

Jia Huang[1] · Xin Tong[1] · Jiacao Yang[1] · Zhao Wang[1] · Meilin Zhang[2] · Xiaojun Wang[2,3] · Jie Yang[2,4]

Received: 16 February 2020 / Accepted: 16 April 2020 / Published online: 7 May 2020

Abstract
In this study, poly (hexamethylene terephthalamide)-co-polycaprolactam (PA6T/6) /organic montmorillonite (OMMT) composites were synthesized through melt-blending and in-situ polymerization. The interlamellar spacing of the montmorillonite in the composites prepared by in-situ polymerization (iPM) is larger than that of those composites prepared by melt-blending (mPM) shown in X-ray diffraction (XRD) curve, indicating intercalation of clay occurred in iPM composites. The morphology of mPM composites and iPM composites were observed taking advantage of scanning electron microscopy (SEM) and transmission electron microscopy (TEM). Both methods reveal that well-organized intercalation and exfoliation structure were formed in iPM composites while the clay in mPM composites tends to self-aggregate, which corresponded well with the XRD results. In violent contrast to mPM composites, the tensile strength of iPM composites was largely increased to 95.1 MPa with 1 wt% of OMMT content compared to that of the neat PA6T/6 (69.8 MPa). In addition, the water absorption is also alleviated by 26.8% at room temperature (23 °C) and 23.6% at high temperature (90 °C) for iPM composites while no obvious difference is observed for mPM composites, which is in consistent with the results of water vapor transmission rate.

Keywords Montmorillonite · In-situ polymerization · Tensile strength · Water absorption

Introduction

Polymer/clay nanocomposites, a classic solution to the improvement of mechanical, thermal and flame-retardant properties of polymeric materials, has been well studied since the end of last century [1]. Owing to its easy availability, well known intercalation/exfoliation chemistry, large surface area and high surface reactivity, montmorillonite (MMT) has become one of the most popular candidates in preparation of polymer nanocomposites [2–4]. However, most of the coiled hydrophobic macromolecules are reluctant to penetrate into the interlayer of the pristine MMT due to the hydrophilic property and small interlayer spacing of inorganic particles [5, 6]. In order to overcome this dilemma, the modified MMT was invented and played a critical role in helping the nanoparticles to expand, separate and exfoliate in matrix, which weaken the interlayer cohesive energy and form a more compatible system [7, 8]. As a result, various modified montmorillonites have been industrialized and applied to the polymer, such as Cloisite®6A, Cloisite®10A [9], Cloisite®15A [10], Cloisite®93A and Cloisite®30B [11, 12].

It is widely accepted that the ability to incorporate clay nanoplatelets into a polymeric matrix with a high level of exfoliation and orientation is a crucial factor which affects the comprehensive properties of nanocomposites [13]. Basically, there are two traditional methods to obtain nanocomposites: melt intercalation and solution intercalation [14]. Regardless of the dispersion medium and blending temperature it may differ, direct dispersion of polymer and layered montmorillonite

✉ Xiaojun Wang
wangxj@scu.edu.cn

[1] College of Polymer Science and Engineering, Sichuan University, Chengdu 610064, People's Republic of China

[2] Analytical and Testing Center, Sichuan University, Chengdu 610064, People's Republic of China

[3] State Key Laboratory of Organic–Inorganic Composites, Beijing 1000294, People's Republic of China

[4] State Key Laboratory of Polymer Materials Engineering, Sichuan University, Chengdu 610065, People's Republic of China

is hard to obtain uniform nanocomposites, especially for the rigid polymeric framework. In-situ intercalative polymerization, a relatively new approach to disperse inorganic clay, could effectively tackle with this problem. Therefore, there have been successive studies on the preparation of polymer/clay nanocomposites by in-situ polymerization. For instance, Q H Zeng et al. [15] reported the synthesis of highly ordered single layered polyaniline/clay composites by in-situ intercalative polymerization. M.Colonna et al. [16] revealed that montmorillonite modified with an imidazolium salt with two long alkyl chains exhibited wide-d spacing and high thermal stability. In addition, Shan Wu et al. [17] synthesized unsaturated polyester/organic montmorillonite (OMMT) nanocomposites with improved mechanical and thermal properties due to the well-dispersed OMMT in the UP matrix.

Polyamide (Nylon) is currently the most widely used engineering plastic because of its good mechanical properties, high temperature resistance and relatively lower cost. Among various kinds of polyamide, semi-aromatic polyhexamethylene terephthalamide (PA6T) possesses high thermostability and melting processability, which combines the advantages of aromatic and aliphatic ones. Yet the decomposition temperature of PA6T is close to the melting temperature, making it hard to be processed under the practical condition. To solve this problem, copolymerization of aliphatic segments with PA6T, known as PA6T/6, will effectively lower the melting temperature and broaden the process window [18, 19]. For PA6T/6, the mechanical property and water absorption is still inferior to some wholly aromatic polyamide, which is crucial to the dimensional stability as structural material. Therefore, it's our primary concern to design PA6T/6 based nanocomposites with enhanced properties. To the best of our knowledge, organic montmorillonite has not been discussed in PA6T/6 system but it proved to be useful in improving mechanical properties and gas barrier property as nanofiller.

For OMMT based nanocomposites, different intercalation methods have been constantly reported for the past decades, yet very few make a comparison. In regard of this, in this paper two different intercalation methods (melt-extrusion intercalation and in-situ intercalative polymerization) to prepare PA6T/6/OMMT nanocomposites were devised. The copolymerization ratio of PA6T/6 is 50:50, determined by our previous study [20, 21]. Moreover, the morphology and the comprehensive properties of the nanocomposites were discussed systematically.

Experimental

Materials

PA6T/6 (50/50) for melt-extrusion intercalation was supplied by Sanli Benzo New Material Corporation (Qingdao, China). The organically modified clay (I.24TL) was purchased from Nanocor (USA), and the modifier is $HOOC(CH_2)_{17}NH_3^+$. Terephthalic acid was supplied by Sinopec Yangzi Petrochemical Corporation (China). Hexamethylenediamine and caprolactam were obtained from Kelon Chemical Reagent Factory (Chengdu, China).

Preparation of PA6T/6/OMMT nanocomposites

Melt extrusion intercalation Prior to the processing step, PA6T/6 and montmorillonite were dried for more than 24 h at 100 °C to remove moisture. Subsequently, PA6T/6 and organoclay were added in a high-speed mixer to disperse for 10 mins, and then the PA6T/6/OMMT composites were prepared by a twin-screw extruder. The bulk PA6T/6 resin was also extruded and pelleted at the same processing conditions in a twin-screw extruder as comparison. The temperature of each section of the twin-screw extruder is set to 220 °C, 260 °C, 280 °C, 290 °C, 300 °C, 305 °C, 310 °C, 310 °C, 310 °C, 305 °C, respectively. According to the different percentage 0%, 0.5%, 1%, 1.5%, 2%, 3% of OMMT, the obtained PA6T/6/OMMT composites are noted as mPM-0, mPM-0.5, mPM-1, mPM-1.5, mPM-2, mPM-3. The detailed experimental procedure is shown in scheme 1.

In-situ intercalative polymerization Scheme 2 shows the synthetic route of PA6T/6/OMMT nanocomposites with solution-solid phase polycondensation method. The synthetic equation of PA6T/6 is shown in Fig. 1. The typical synthetic procedure for the PA6T/6/OMMT nanocomposites is described as follows. First of all, appropriate amount of caprolactam (CPL), hexamethylenediamine and terephthalic acid were charged in preparation of 50:50 PA6T/6 copolymer. Then, OMMT and CPL were homogeneously dispersed in 600 mL deionized water through an ultrasonic instrument for about 12 h. Subsequently, certain amount of caprolactam, hexamethylenediamine, terephthalic acid and OMMT aqueous solution were transferred to an autoclave and kept at 90 °C for 4 h with vigorous mechanical stirring under nitrogen atmosphere. After that, the temperature of autoclave was continuously raised to 230 °C and maintained for 1 h, and the pressure of reactor would rise to 2.4 MPa. After slowly discharging the gas, 0.5 MPa N_2 was filled in. In the final stage of polymerization, the temperature was raised to 260 °C simultaneously and maintained for 3 h. After completion of the reaction, OMMT/PA6T/6 nanocomposites were taken out and dried under vacuum at 100 °C for at least 48 h. After extrusion and pelleting by twin-screw extruder, those products were noted as iPM-0.5, iPM-1, iPM-1.5, iPM-2, iPM-3 according to the mass fraction of OMMT. Bulk PA6T/6 copolymer (iPM-0) was also synthesized by in-situ polymerization under the same condition free of OMMT.

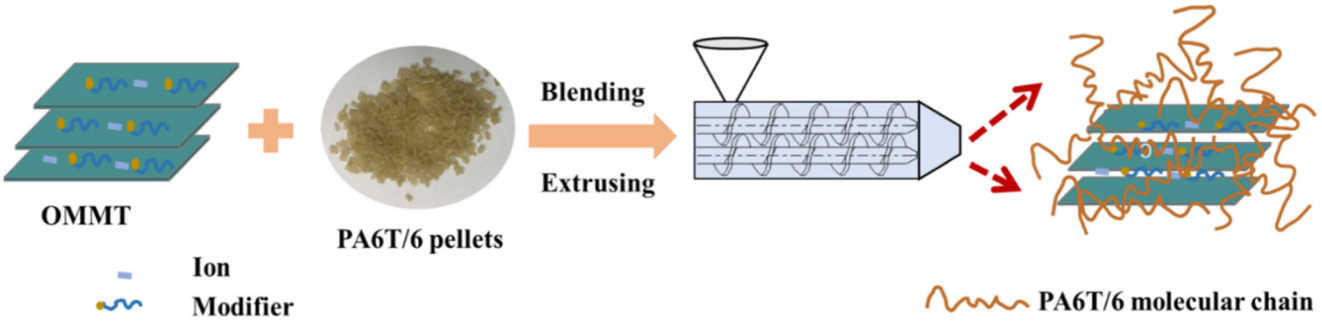

Scheme 1 Preparation of mPM composites by melt extrusion intercalation

Preparation of test specimens

Film specimens for structural characterization (FT-IR and XRD) and performance test (WVTR) were prepared through hot-press molding at 300 °C. The samples for the test of mechanical properties and water absorption (4 cm × 4 cm × 2 mm) were obtained by injection molding and subsequently annealed at 135 °C for 8 h. The parameters of the injection molding process are shown in Table 1.

Characterization

The intrinsic viscosity of free PA6T/6 was obtained at 30 ± 0.1 °C with 0.125 g polymeric powder dissolved in 25 mL concentrated sulfuric acid, measuring by a Cannon-Ubbelodhe viscometer. The values were obtained by the one-point method [22].

Fourier transform infrared spectra (FT-IR) was conducted on a Nicolet 670 spectrophotometer. The samples were spread on a KBr pellet for scanning.

A Bruker-600 NMR spectrometer was used to verify the samples' structure. All test samples were dissolved in trifluoracetic acid-D.

The X-ray diffraction patterns of OMMT/PA6T/6 nanocomposites were investigated on a Philips X' pert Pro MPD X-ray system with angle scanned from 2θ = 5–13° (λ = 0.154 nm) at a voltage of 40 kV and the current of 100 mA.

The images of the impact fractured surface (quenched and broken in liquid nitrogen) were analyzed with a JSM-7500F field emission scanning electron microscope (SEM). All samples were sputtered with a thin layer of gold before observation. Samples for transmission electron microscope (TEM) were cut into ultrathin sections using a diamond knife at about −100 °C. The internal morphology of nanocomposites was performed on a JEOL JEM 100CX II TEM equipment equipped with 120 kV accelerating voltage.

Thermogravimetric analysis (TGA) was carried out under N_2 atmosphere with a TGA Q500 from TA Corporation at a heating rate of 10 °C/min from room temperature to 800 °C.

Differential scanning calorimetric analysis was performed on a Netzsch-201F equipment (Germany) under nitrogen atmosphere to observe the thermal behavior of melting and crystallization. The samples were preheated to 330 °C (10 °C/min) and cooled to room temperature (10 °C/min) to eliminate thermal history before the second heating.

The tensile strength, modulus and elongation at break were measured in accordance with GB/T 1040.2–2006 standard at

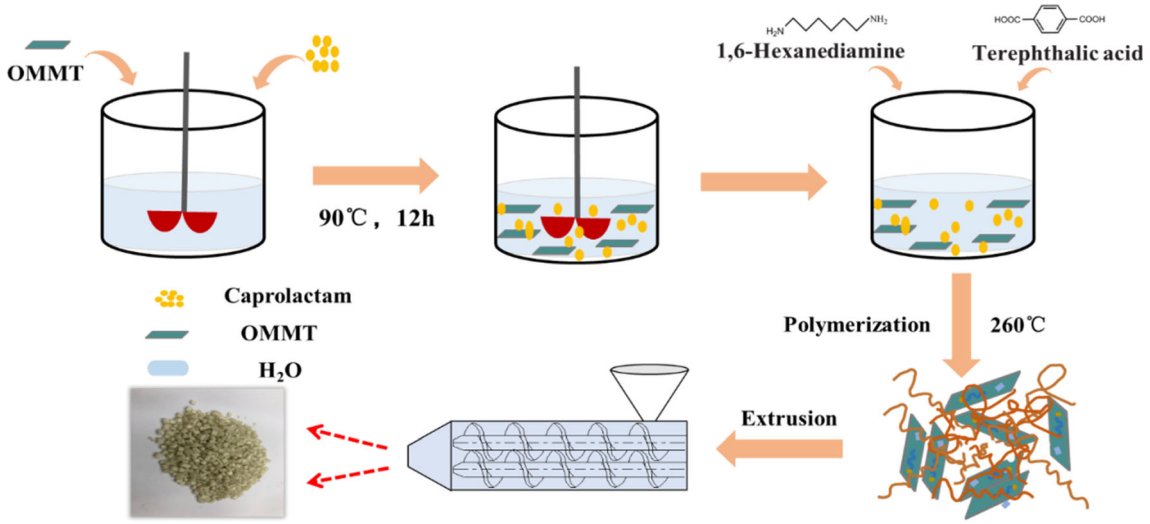

Scheme 2 Preparation of iPM composites by in-situ intercalative polymerization

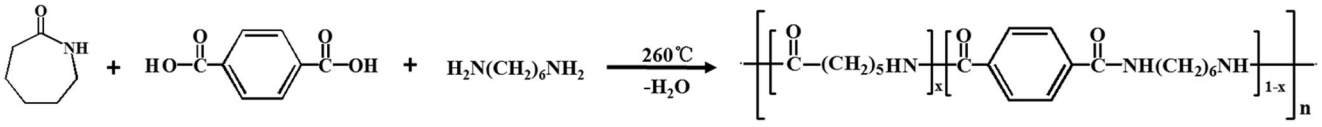

Fig. 1 Synthetic equation of PA6T/6

room temperature with a tensile rate of 10 mm/min. Flexural strength test was conducted according to GB/T 9341–2008 with a loading rate 2 mm/min. At least eight specimens were employed for each sample in the mechanical test.

Water vapor transmission rate (WVTR) measurements were conducted according to the GB/T 21529–2008 standard, using a WVTR-901R instruments under the condition of 23 °C and 85% RH. Three film specimens were employed for each group of samples in the WVTR tests.

The water absorption content of nanocomposites was carried out under the same standard in which the OMMT/PA6T/6 specimens (4 cm × 4 cm × 2 mm) for water absorption measurement were dried at 100 °C in a vacuum oven until a constant weight (W_0) was attained. Then, the samples were fully immersed in water at 23 °C and 90 °C. Weight gains were recorded by taking out the samples and wiping off excess water from the surface of the samples after 24 h soaking. At least six specimens were employed for each group of samples in the water absorption tests. Water absorption was calculated according to the following equation:

$$Mt(\%) = \frac{\text{Wd-W0}}{\text{W0}} \times 100\% \quad (1)$$

Where W_0 and W_d represent the initial weight of samples and the weight of samples after soaking, respectively.

Results and discussion

Chemical structure

The FT-IR spectra of PA6T/6 (iPM-0) and iPM-2 were recorded and shown in Fig. 2. In the spectra, the peaks near 2935 cm^{-1} and 2872 cm^{-1} are contributed to the absorption peak of -CH_2-. The peaks near 1623 cm^{-1} and 1524 cm^{-1} correspond to the stretching vibration of C=O and bending vibration of N-H respectively. The peaks near 830 cm^{-1} were the characteristic absorption of benzene ring. The above results demonstrate the formation of amide products with benzene ring. The characteristic peaks of two curves are almost the same, which indicates small amount of montmorillonite may not bring much change to FT-IR spectra of PA6T composites. ^{1}H-NMR spectrum of PA6T/6 copolymer was illustrated in Fig. 3. The peak (a) near 8.3 ppm in the spectra was attributed to the aromatic protons. The chemical shifts at 2.92 (c), 1.97 (d), 1.71 (e), and 1.90 (f) ppm were belonged to the aliphatic protons. The proton signal peak next to 4 ppm was split into two adjacent parts, on behalf of the protons of 6 T (b_1) and 6 (b_2) units respectively. The foregoing results suggest that the PA6T/6 copolymers were successfully synthesized via polymerization described in Scheme 2. The actual ratio of 6 unit and 6 T unit was close to 1:1.2, calculated by integration. Small deviation from theoretical value (1:1) may be due to the volatilization of CPL at high temperature.

Inherent viscosity of free PA6T/6

The inherent viscosity (η) of free PA6T/6, one important indicator to molecular weight, was summarized in Table 2. The viscosity of the mPM was measured as 0.899 dL/g, whereas the viscosity of the iPM composites decreased with the increasing fraction of OMMT. On the one hand, such fall could be ascribed to the amino hexadecanoic acid group in the modified OMMT. The carboxylic acid group in clay, though in tiny amounts, disrupted classic 1:1 polycondensation ratio and impeded the growth of polyamide molecular segments. On the other hand, the existence of clays increased the barrier properties of composites and decelerated the removal of water from the reaction mixture, which undoubtedly impacted the reaction rate and degree of polymerization [23]. Despite disadvantages discussed above, the inherent viscosity of OMMT/PA6T/6 was higher than 0.6 even for 3 wt% content of OMMT. That implied high molecular weight PA6T/6 was obtained through the method of in-situ intercalative polymerization.

Characterization of nanostructure

Small angle XRD analysis in Fig. 4 was used to distinguish the extent of intercalation and exfoliation from the distance of (001) crystal plane, which was calculated according to

Table 1 Parameters of the injection molding process

first stage temperature (°C)	second stage temperature (°C)	third stage temperature (°C)	injection pressure (%)	injection speed (%)	injection time (s)
310	310	290	50	50	15

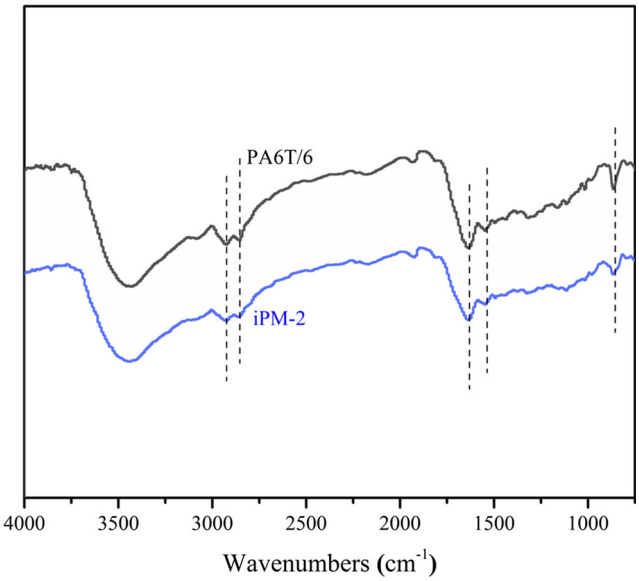

Fig. 2 the FT-IR spectrum of PA6T/6 (iPM-0) and iPM-2

Bragg's law ($d = \lambda/2\sin\theta$) [24]. That is, the lower of diffraction angle, the higher of interplanar spacing. For mPM, the characteristic diffraction peak is observed at $2\theta = 7.13°$, with a basal distance of 1.24 nm (the basal distance of MMT is about 1.2 nm), indicating the aggregation and rare intercalation occurred during the melting blend. However, the diffraction peak of iPM shifted to a lower angle at $2\theta = 6.03°$ corresponding to an interlayer spacing of 1.45 nm. The increased spacing confirms that the clay was rather well intercalated in iPM than mPM. There is no diffraction peak observed for iPM-0.5 and iPM-1, which indicated that the full exfoliation of clay layers in the PA6T matrix. For iPM, it should be noted that almost similar XRD curves ($2\theta = 6.08^{\circ}$) are obtained when the content of clay was higher than 1 wt%, which implied that good intercalation could be reserved even for slightly excessive filler content.

Table 2 The intrinsic viscosity of PA6T/6 with different content of clay prepared by melt intercalation and in-situ intercalative polymerization

Content of Clay (wt%)		0	0.5	1	1.5	2	3
Viscosity	mPM	0.899					
	iPM	0.926	0.878	0.812	0.759	0.716	0.635

SEM and TEM images of the composites (mPM and iPM) are combined to evaluate the dispersion of clays in PA6T/6. As shown in Fig. 5b and Fig. 5c, extensive aggregation of clay could be observed for mPM-1 composites while no distinct aggregation structure is found for iPM-1 composites. What's more, the SEM images of iPM-1 show that the interface between filler and matrix was smooth, and no obvious interfacial defect were detected, which verified better dispersion of nanofiller for in-situ intercalative polymerization.

TEM was applied to further investigate the internal structure of prepared OMMT/PA6T/6 composites. Figure 5e shows exfoliation of montmorillonite for iPM-1, but for mPM-1, bulky agglomerate with a size of about 200 nm was observed, which is in agreement with the XRD and SEM results. The above results indicate that nanocomposites with well-dispersed fillers have been attained by in-situ polycondensation where polymerization occurred subsequently with the intercalation of monomer into the OMMT interlayer.

Thermal properties

The effect of OMMT on the thermal decomposition temperature of iPM samples was analyzed by TGA analysis. The

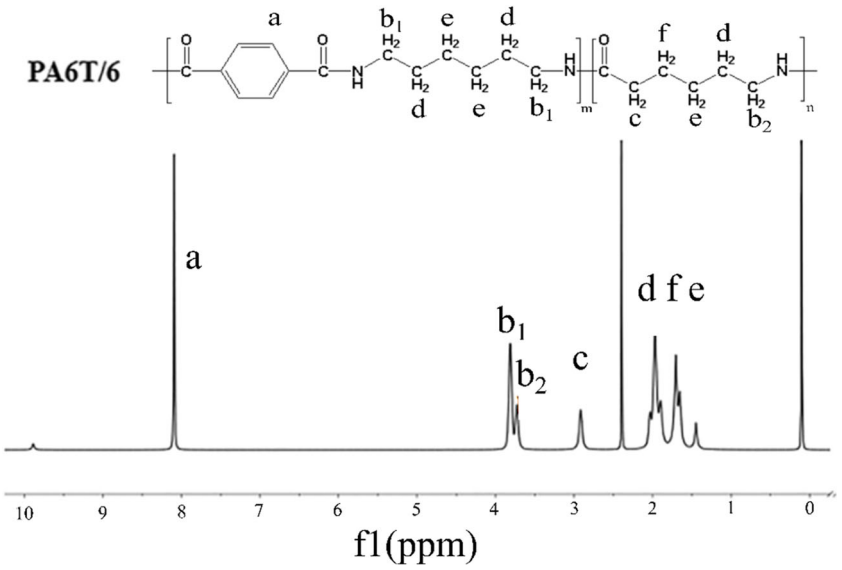

Fig. 3 the ^{1}H-NMR spectrum of PA6T/6 50/50 (iPM-0)

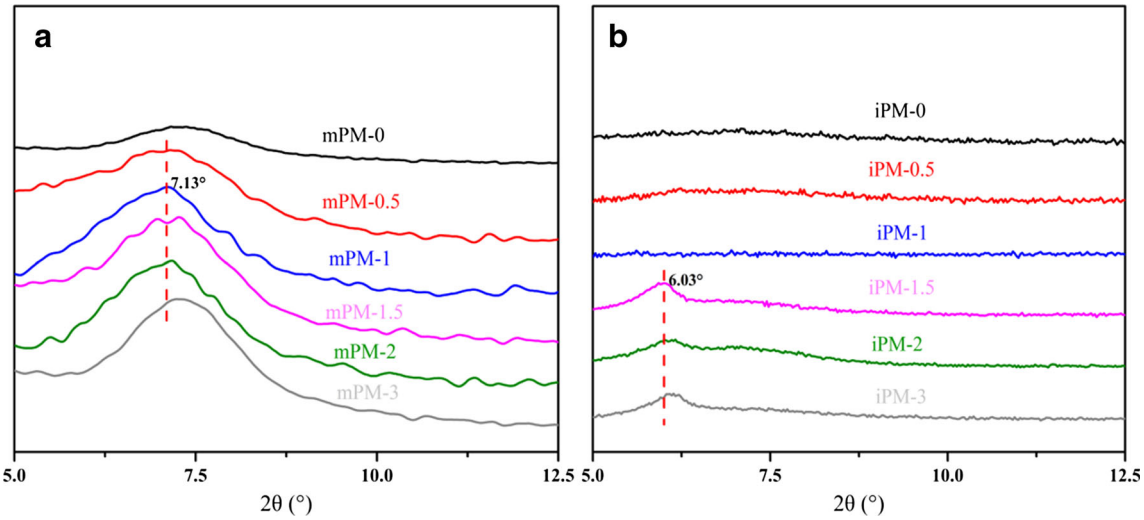

Fig. 4 XRD curves of mPM and iPM composites: (**a**) mPM composites, (**b**) iPM composites

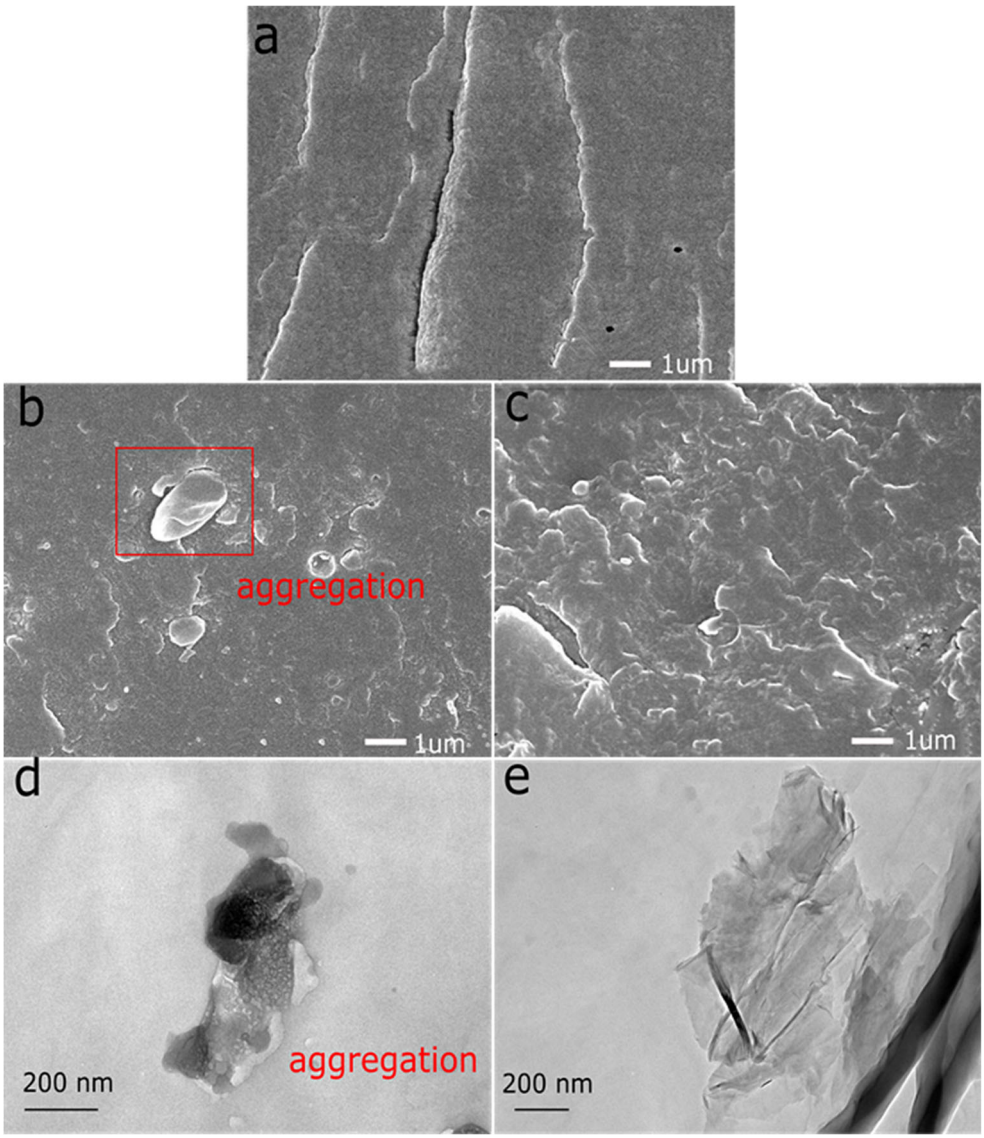

Fig. 5 SEM images of (**a**) bulk PA6T/6; (**b**) mPM-1 composite; (**c**) iPM-1 composite; TEM image of (**d**) mPM-1 composite; (**e**) iPM-1 composite

Table 3 Summary of thermal data of iPM composites

Content of Clay (wt%)	T_d (°C)	T_m (°C)	T_c (°C)	T_g (°C)	ΔH_m (J/g)	ΔH_c (J/g)
0.0	376.3	292.9	254.3	99.9	−49.6	43.1
0.5	382.0	287.5	247.4	103.9	−39.9	33.7
1.0	386.1	288.9	251.6	98.4	−51.2	39.3
1.5	387.6	291.0	249.7	101.7	−58.7	40.6
2.0	389.0	293.7	252.2	102.6	−19.7	31.4
3.0	391.2	294.1	254.7	99.0	−11.7	28.5

temperature of 5% weight loss ($T_{5\%}$) was employed to evaluate the thermal stability of the materials (Table 3). As shown in Fig. 6, the $T_{5\%}$ of iPM-0.5, iPM-1, iPM-1.5, iPM-2 and iPM-3 rises by 5.7, 9.8, 11.3, 12.7, and 14.9 °C, respectively, compared to the bulk resin (iPM-0). This phenomenon is probably related to the fact that the barrier property of well-dispersed OMMT prohibit the escape of volatile during the thermal degradation process [25].

Figure 7 shows the DSC curves of iPM composites with different contents of OMMT, the glass transition temperature (T_g), the melting temperature (T_m), the crystallization temperature (T_c) are summarized in Table 3. With lower content of OMMT, the crystallization temperature and the melting temperature of the nanocomposites were almost unchanged. But with a higher content of filler, both of the crystallization and the melting peak diminished. That is mainly due to the fact that high content of nanoparticles restricted the molecular chains from rearrangement into crystallized phase during the cooling process [26]. It could be further verified by the crystallization enthalpy and the melting enthalpy of the samples. There is no obvious change when the filler content is below 1.5 wt%. However, the crystallization enthalpy falls from −58.7 J/g to −11.7 J/g, in line with the melting enthalpy from −40.6 J/g to −28.5 J/g when OMMT content increases to 3 wt%. Moreover, the content of OMMT is believed to be no more relevant when it comes to glass transition temperature (T_g), as shown in Fig. 7a. Generally speaking, minor addition of inorganic filler exerts limited influence on the free volume of macromolecules [27]. For PA6T/6/OMMT composites system, compared to the bulk resin, the float value of T_g is below 4 °C.

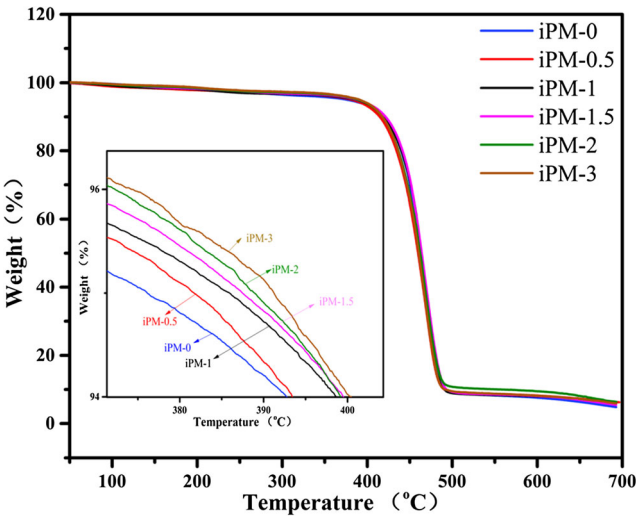

Fig. 6 TGA curves of iPM composites with different OMMT content

Mechanical properties

In order to evaluate the effects of OMMT on mechanical properties, the tensile strength and the flexural strength of the composites were measured, which are illustrated in Fig. 8 and Table 4. As shown in Fig. 8a, the tensile strength of the mPM composites first increased and then decreased with the increase of OMMT content. It reached maximum at 0.5 wt% OMMT content, and the tensile strength of the composite was 79.0 MPa (increased by 8.97% compared to mPM-0), while dropped considerably by higher OMMT incorporation. That's mainly due to the poor dispersion of OMMT in matrix for mPM series, which was in consistent with the XRD and TEM results. Similar trend was observed for the strength modulus of mPM composites (Fig. 8b). The OMMT nanosheets tend to extensively stack in mPM composites prepared by melt-blending, serving as stress concentration and weakening the effect of nano reinforcement. However, as shown in Fig. 8a, in comparison with bulk PA6T/6 (iPM-0), the tensile strength of iPM-0.5, iPM-1, iPM-1.5 and iPM-2 was increased by 30%, 36.2%, 31.9% and 20.9% respectively. It was noteworthy that the tensile strength of in-situ polymerized OMMT/PA6T/6 composites could be up to 95.1 MPa, close to some reported wholly aromatic polyamide [28, 29]. Unlike the tensile strength, the tensile modulus of all surveyed composites (Fig. 8b) were in the range of 3.5–4 GPa, suggesting the stiffness of composites were more depending on the bulk resin for low content of nanoparticles. Figure 8c showed the elongation at break of mPM and iPM composites. Not surprisingly, iPM composite outweighed its counterpart in all surveyed OMMT concentration. The degree of dispersion again played an essential role in reserving the toughness of nanocomposites. In addition, in comparison with PA6T/6, the flexural strength of iPM composites and mPM composites increased by 57.5% and 44.8% respectively (Fig. 8d). The

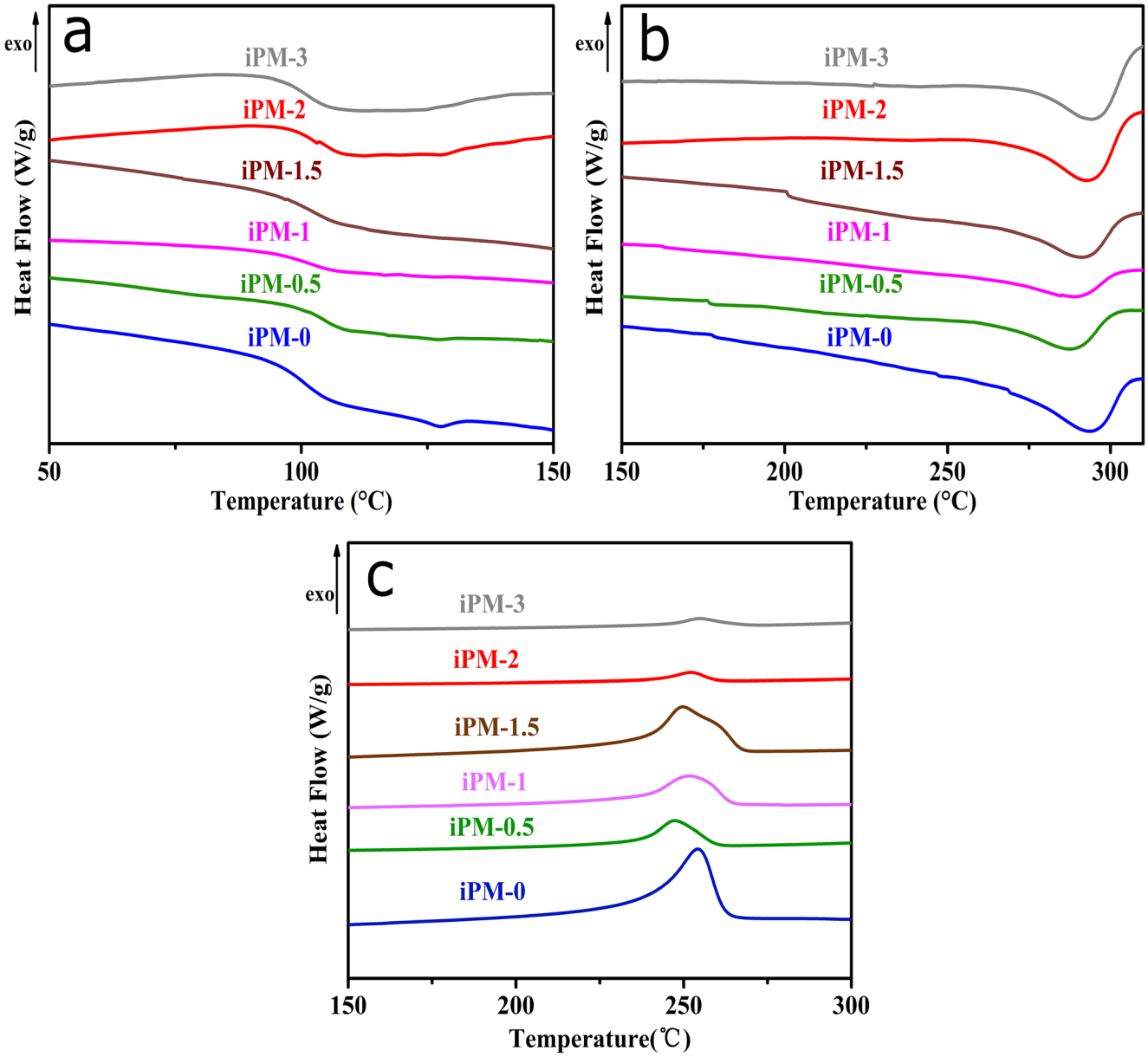

Fig. 7 the DSC curves of iPM composites with different OMMT content: (**a**) secondary heating curve (50–150 °C), (**b**) secondary heating curve (150–310 °C), (**c**) cooling curve

improvement of the mechanical properties of composites is attributed to the high aspect ratio and high modulus of montmorillonite. Obviously, the different state of OMMT in nylon matrix (aggregation, intercalation or exfoliation) and interface adhesion between clay and polymer can explain the difference in mechanical properties for mPM and iPM composites.

Water vapor transmission rate (WVTR) testing

The WVTR values of different PA6T/6 composite films are compared in Fig. 9. As a result, the WVTR of the iPM composites decreased from 1.41 g/m^2·day to 1.04 g/m^2·day, which is attributed to the fact that OMMT efficiently blocks the penetrating passage of the water molecules. The WVTR improvement could be up to 27% and it's better than the reported PLA/Chitosan/Clay system (14% improved WVTR) [30]. In the case of mPM composites, the WVTRs of mPM films show little difference from that of the bulk resin, indicating that the barrier performance is highly related to the dispersion of OMMT. Figure 10 presents a schematic diagram of water molecules passing through the composites.

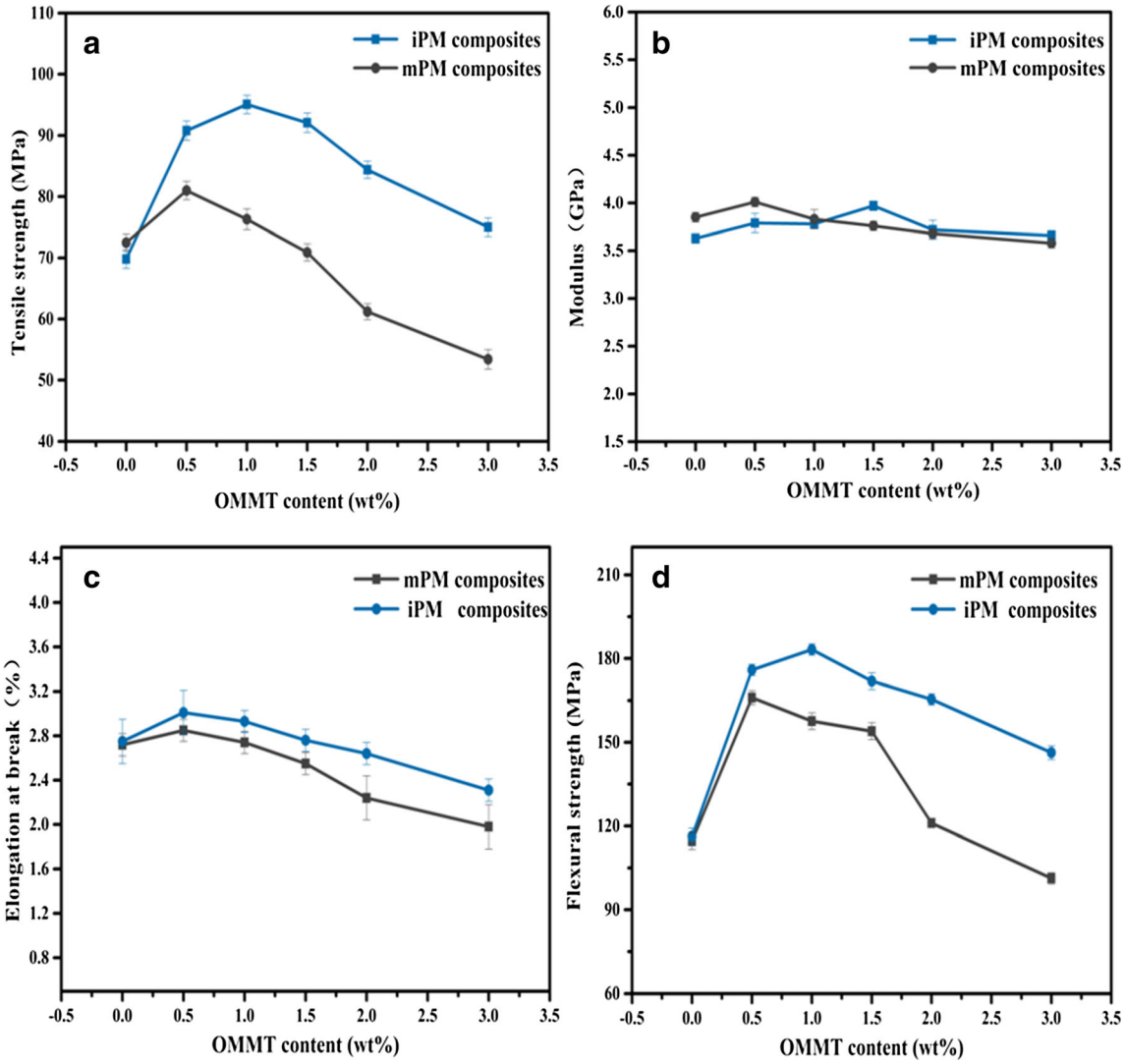

Fig. 8 Mechanical properties of mPM and iPM composites with different OMMT concentration (**a**) tensile strength (**b**) tensile modulus (**c**) elongation at break (**d**) flexural strength

Water absorption of composites

Dimensional stability is strongly affected by the water absorption, which is especially important for nylon. Amide group in polyamide makes it a hydrophilic engineering plastic and the water absorption of nylon needs to be restricted before put into use as structural material. Montmorillonite has been widely applied to enhance the

Table 4 The data of mechanical properties of mPM and iPM composites

Clay Content (wt%)	Tensile Strength (MPa)		Tensile Modulus (GPa)		Elongation at Break (%)		Flexural Strength (MPa)	
	mPM	iPM	mPM	iPM	mPM	iPM	mPM	iPM
0.0	72.5	69.8	3.85	3.63	2.72	2.75	114.6	116.3
0.5	81.0	90.8	4.01	3.79	2.85	3.01	166.0	175.9
1.0	76.3	95.1	3.83	3.78	2.74	2.93	157.6	183.2
1.5	70.9	92.1	3.76	3.97	2.55	2.76	154.0	171.9
2.0	61.2	84.4	3.68	3.72	2.24	2.64	121.0	165.4
3.0	53.4	75.0	3.58	3.66	1.98	2.31	101.3	146.3

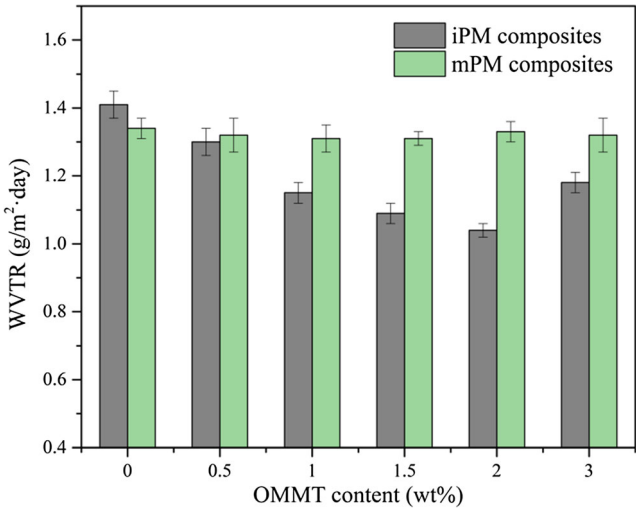

Fig. 9 The WVTR values of mPM and iPM composites with different OMMT contents at 23 °C and 85% RH

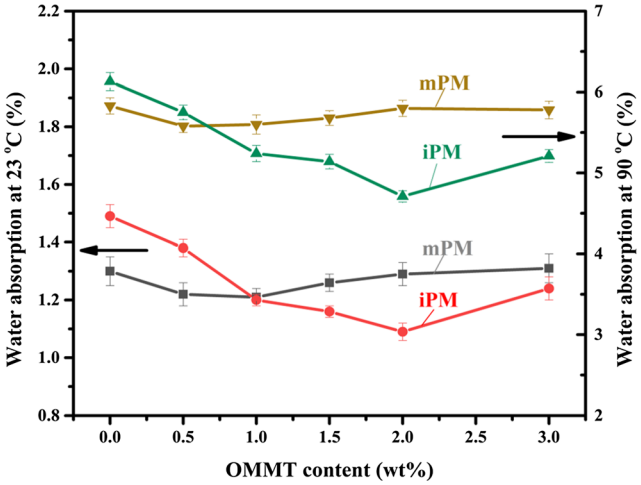

Fig. 11 The water uptake of mPM and iPM composites with different OMMT concentration at 23 °C and 90 °C in 24 h

gas barrier property and lower water absorption rate of composites. In fact, the morphology and dispersion of clay sheets in polymer matrix are the key factors to water barrier properties [31]. The water absorption values were summarized in Fig. 11, both for mPM and iPM samples. No distinguished improvement was observed for mPM composites at 23 °C and 90 °C which is consistent with the result of WVTR test. The water uptake largely increases at 90 °C for the faster movement of water molecule and looser structure of molecular chains at higher temperature, since the glass transition temperature of PA6T/6 was in the range of 98–104 °C. Compared with the mPM composites, the iPM composites exhibited a reduction rate of 26.8% and 23.2% at 23 °C and 90 °C respectively. That is contributed to the improved barrier properties in iPM composites. Though the bulk resin of mPM series exhibited lower water absorption than home-made iPM ones due to the commercial end-capping reagent, in-situ intercalation induced iPM-1.5 and iPM-2 composites outperformed all mPM composites regardless of the content of fillers and the test temperature. The in-situ intercalation structure characterized by the high specific surface area of the layered OMMT structure blocks the route of water molecule and hinders the diffusion. What's more, the formation of the intercalation structure can also reduce the water uptake, which is contributed

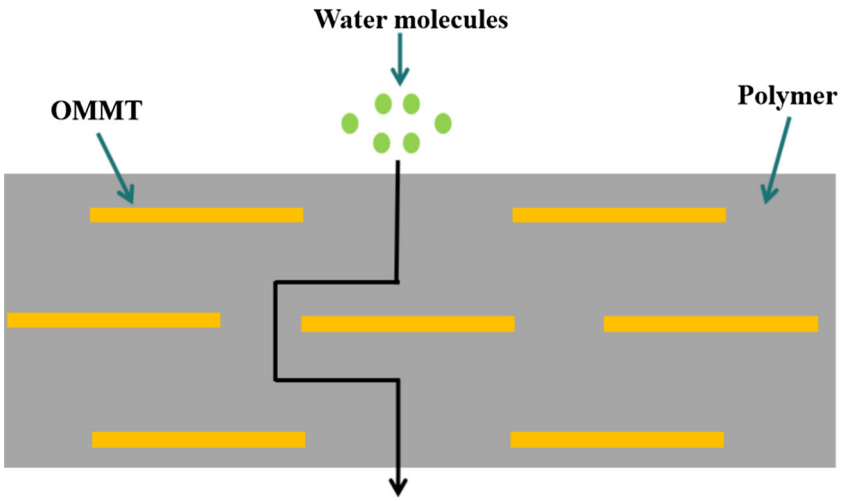

Fig. 10 The schematic diagram of water passing through PA6T/6 composites

to the fact that the absorptive amide bond was shield by growing through the interlayer of OMMT. In short, better dispersion of clay and improved barrier property in iPM composites result in lower water absorption.

Conclusions

The PA6T/6/OMMT composites had been successfully prepared by melt-blending and in-situ polymerization in this paper. The chemical structures, micro structure, thermal properties, mechanical performance, barrier properties and water absorption were investigated and discussed. It has been found that the dispersion of the clay imposed an outstanding effect on the comprehensive performance of PA6T/6 based nanocomposites. To be more specific, the iPM composites synthesized via in-situ polymerization are better intercalated and dispersed, which promotes the mechanical properties, thermal behavior, barrier property and decreases the water uptake at the same time. However, there are no obvious improvement for mPM composites due to the poor dispersion of clay, both observed by XRD, SEM and TEM images. On the one hand, study in this paper proved in-situ intercalative polymerization a better option in dispersing nanofiller in polymeric matrix, especially for the rigid semi-aromatic PA6T/6. On the other hand, organically modified montmorillonite (OMMT), through appropriate method, was believed to nano-enhance the mechanical properties and water absorption of PA6T/6, therefore making it a more promising candidate for the prospective industrial and daily needs.

Acknowledgements The authors gratefully acknowledge the financial support from the Key R&D projects of Jiangsu Province (Grant No. BE2019008) and the Natural Science Foundation of China (Grant No. 51573103, 21274094 and 21304060).

References

1. Kotal M, Bhowmick AK (2015) Polymer nanocomposites from modified clays: Recent advances and challenges. Prog Polym Sci 51:127–187
2. Cui Y, Kumar S, Rao Kona B, Houcke D (2015) Gas barrier properties of polymer/clay nanocomposites. RSC Adv 5:63669–63690
3. Okamoto M (2006) Recent advances in polymer/layered silicate nanocomposites: an overview from science to technology. J Mater Sci Technol 22:756–779
4. Hu X, Ke YC (2020) The influence of organic modified montmorillonite on the solution properties of copolymer containing β-cyclodextrin. J Polym Res 27:19
5. Kiliaris P, Papaspyrides CD (2010) Polymer/layered silicate (clay) nanocomposites: An overview of flame retardancy. Prog Polym Sci 35:902–958
6. Bee SL, Abdullah MAA (2008). Prog Polym Sci 85:57–82
7. Kim TH, Jhon MS (2002) Synthesis and Rheology of Intercalated Polystyrene/Na+-Montmorillonite Nanocomposites. Macromol Rapid Comm 23:191–195
8. Móczó J, Pukánszky BJ (2008). Ind Eng Chem 14:535–563
9. Li X, Ha CS (2001) Preparation and Characterization of Poly(butyleneterephthalate)/Organoclay Nanocomposites. Rapid Comm 22:1306–1312
10. Bhattacharya M, Maiti M, Bhowmick AK (2009) Tailoring properties of styrene butadiene rubber nanocomposite by various nanofillers and their dispersion. Polym Eng Sci 49:81–98
11. Datta H, Singha NK, Bhowmick AK (2008) Beneficial Effect of Nanoclay in Atom Transfer Radical Polymerization of Ethyl Acrylate: A One Pot Preparation of Tailor-Made Polymer Nanocomposite. Macromolecules 41:50–57
12. D'Amico DA, Cyras VP (2012) Crystallization behavior of poly(3-hydroxybutyrate) nanocomposites based on modified clays: Effect of organic modifiers. Thermochim Acta 544:47–53
13. Kong Q, Zhang J (2017) Improving flame retardancy of IFR/PP composites through the synergistic effect of organic montmorillonite intercalation cobalt hydroxides modified by acidified chitosan. Appl Clay Sci 146:230–237
14. Madhumitha G, Thakur VK (2018) Recent advances in starch–clay nanocomposites. Int J Polym Anal Ch 23:331–345
15. Zeng QH, Lu GQ (2002) Synthesis of polymer montmorillonite nanocomposites byin situintercalative polymerization. Nanotechnology 13:549–553
16. Colonna M, Acquasanta F (2017) Effect of telechelic ionic groups on the dispersion of organically modified clays in bisphenol A polycarbonate nanocomposites by in-situ polymerization using activated carbonates. Express Polym Lett 11:396–405
17. Wu S, Zhou Y (2017) Unsaturated polyester/montmorillonite nanocomposites with improved mechanical and thermal properties fabricated byin situpolymerization. J Appl Polym Sci 134:45251
18. Zhang G, Yang J (2016) Effects of a trans- or cis-cyclohexane unit on the thermal and rheological properties of semi-aromatic polyamides. Polym Chem 7:44–53
19. Zhang G, Yang J (2014) Semiaromatic polyamides containing ether and different numbers of methylene (2–10) units: synthesis and properties. RSC Adv 4:63006–63015
20. Wang Z, Yang J (2019) Improved strength and toughness of semi-aromatic polyamide 6T-co-6(PA6T/6)/GO composites via in situ polymerization. Compos Sci Technol 175:6–17
21. Peng WM, Yang J (2018) Semiaromatic polyamide poly(hexamethylene terephthalamide)-co-polycaprolactam: Thermal and flame-retardant properties. J Appl Polym Sci 135: 46451
22. Xu S, Li G (2005) Synthesis and characterization of poly(p-phenylene sulfide sulfone/ketone) copolymer. Polym Bull 54: 251–261
23. Colonna M, Celli A (2017) Effect of telechelic ionic groups on the dispersion of organically modified clays in bisphenol A polycarbonate nanocomposites by in-situ polymerization using activated carbonates. Express Polym Lett 11:396–405
24. Han B, Shen J (2003) Preparation and characterization of nylon 66/montmorillonite nanocomposites with co-treated montmorillonites. Eur Polym J 39:1641–1646
25. Wang X, Kalali EN, Wang DY (2015) An in situ polymerization approach for functionalized MoS2/nylon-6 nanocomposites with

enhanced mechanical properties and thermal stability. J Mater Chem A 3:24112–24120
26. Park SH, Park HJ (2012). Appl Polym Sci 125:675–680
27. Klono P, Kyritsis A (2010) Interaction of poly(ethylene glycol) with fumed silica and alumina/silica/titania. Surface A 360:220–231
28. Zhang G, Yang J (2013) Synthesis and properties of polyamides derived from 4,6-bis(4-chloroformylphenylthio)pyrimidine and 3, 6-bis(4-chloroformylphenylthio)pyridazine. Polym Int 62:1358–1367
29. Zhang G, Yang J (2012) Effects of thioether content on thermal and optical properties of polyamides. Polym Int 61:800–809
30. Kugge C, Vanderhoek N, Bousfield DW (2011) Oscillatory shear response of moisture barrier coatings containing clay of different shape factor. Interf Sci 358:25–31
31. Jalalvandi E, Ilbeygi H (2013). J Thermoplast Compos 28(4):496–509